



# Final Technical Report of AFOSR Grant No. AFOSR-91-0420

## Development of Si Light Emitting Technology Based on Si Quantum Wires

by

Dim-Lee Kwong

*Microelectronic Research Center  
Department of Electrical and Computer Engineering  
University of Texas at Austin, Austin, TX 78712*

Accession For	
NTIS CRA&I	<input checked="" type="checkbox"/>
DTIC TAB	<input type="checkbox"/>
Unannounced	<input type="checkbox"/>
Justification	
By	
Distribution /	
Availability Codes	
Dist	Avail and/or Special
A-1	

### Table of contents:

1. Objectives .....	1
2. Process Development.....	2
3. Material Study .....	3
4. PL Mechanism Study.....	4
5. EL Devices.....	7
5.1 Device Fabrication .....	7
5.2 Device Characterization .....	8
6. Conclusions .....	8
7. References .....	10
8. Publication Lists .....	12
Figures and Captions .....	14

19950615 053

# **Final Technical Report of AFOSR Grant No. AFOSR-91-0420**

**Dim-Lee Kwong**

*Microelectronics Research Center, Department of Electrical and Computer Engineering  
The University of Texas at Austin, Austin, TX 78712*

## **1. Objectives**

The recent observation that porous Si (PS), which was previously known to exhibit visible photoluminescence (PL) at 4.2 K [1], also exhibit relatively intense visible PL at room temperature [2] has attracted considerable attention and encouraged prospects of Si-based optoelectronics. The development of a Si light-emitting source would be able to tap into the relatively mature Si technology and would mark a major breakthrough for display, optical interconnects, telecommunications, *etc.*

The objectives of this program are four folds. (I) Process development: develop new techniques to fabricate luminescent PS, control the luminescence spectra, and process PS with minimal damage to the luminescent properties. To that end, we have developed a novel approach to produce luminescent PS without an external electrical bias by stain etching Si in HF-HNO<sub>3</sub>-based solution [3,4]. In addition, we have utilized dry oxidation to efficiently control the PL spectrum. Excellent PL selectivity with micrometer resolution was also achieved by protecting Si with a metal or dielectric mask during anodization. (II) Material study: characterize the microstructure and physical chemistry of luminescent PS as functions of preparation conditions by microscopic and spectroscopic techniques. (III) PL mechanism study: investigate the origin of visible PL in PS by studying quantum-size effects, H-based models, molecular electronics, as well as the effects of surface passivation. (IV) Electroluminescence (EL) devices: fabricate and characterize the PS-based EL devices. Surface-emitting and edge-emitting light-emitting diodes (LEDs) have been fabricated and critically characterized. The rest of this report will address the mentioned objectives point by point to demonstrate the significant contributions made in this study.

## 2. Process Development

PS is usually made by anodizing bulk Si in HF-based electrolyte. The anodization is an electrochemical process, in which the Si sample serves as the anode and is connected to the positive polarity of an external power source. However, the production of PS by anodization sometimes causes processing difficulties. For instance, structures containing high-impedance materials, such as in silicon-on-insulator (SOI) or undoped Si, cannot be conventionally anodized through the backside contacts due to lack of a conducting pathway.

The discovery of a novel approach to fabricate PS by stain etching in our study serves to solve the above problem. By chemical etching Si in HF-HNO<sub>3</sub>-H<sub>2</sub>O solutions without the need of any external power supply, we first time showed that the resulting stained PS was visibly luminescent at room temperature with the intensity comparable to anodized PS within an order of magnitude deviation [3]. The formation of PS by this approach was explained in terms of a result of electrochemical reactions, in which a number of excess holes and electrons are generated and they subsequently dominate the porous film formation.

The modulation of PL spectra of PS can be readily obtained by dry oxidation if the quantum-size effect dominates the luminescence mechanism [5]. The PL spectrum is modulated in both intensity and emission energy after the dry oxidation, which serves to change the sizes and volume of the luminescent Si particles. As shown in Fig. 1 is the PL evolution of a weakly luminescent PS sample with 53% porosity after it is oxidized at 700°C in diluted oxygen. The PL can be shifted into visible range with a dramatic increase in intensity within a minute. The efficiency of such control is much better than quiescent immersion of the PS sample in HF solution [2], in which case it takes hours to achieve the same effect.

With the probability of integrating PS into conventional Si processes, we investigate the selective area formation of luminescent PS by masking the Si sample with a variety of materials, including SiO<sub>2</sub>, Si<sub>3</sub>N<sub>4</sub>, Pt, and PtSi<sub>2</sub>. Among these masking materials, plasma-enhanced chemical vapor deposition (PECVD) Si<sub>3</sub>N<sub>4</sub> shows promise for the application of selective formation of luminescent PS. A layer of 100 Å-thick pad oxide was grown before the deposition of 5 μm-thick Si<sub>3</sub>N<sub>4</sub> to reduce the film stress. After standard photolithographic patterning, the exposed Si

was anodized to luminescence with the masked Si intact. Pattern dimensions investigated ranged from 4  $\mu\text{m}$  to 1000  $\mu\text{m}$ , and included line, array, and pitch patterns. An example of the resulting microPL imaged by focused 488 nm laser is demonstrated in Fig. 2. The PL appeared solid and quite uniform under the microscope. The PECVD nitride can be readily removed by prolonged etching in HF-based solution with minimal perilous effect on the formed luminescent areas.

### 3. Material Study

A variety of spectroscopic and microscopic techniques have been utilized to characterize luminescent PS in this study. Fourier-transformed infrared spectroscopy (FTIR) was primarily used to monitor the change in O, C, H, and F contents during varied processing of PS. It is shown by FTIR that the fresh as-anodized PS is passivated by H, with negligible amount of O and C appearing in the spectrum. In order to study the fragile structure of luminescent PS, a novel sample preparation procedure for transmission electron microscopy (TEM) was proposed to avoid preparation artifacts [6]. The formation of PS is scheduled as the last step in the new procedure, instead of the first one as in the conventional TEM sample preparation sequence. The new procedure can reduce the possibility of the artifacts introduced during the mechanical polishing, solvent cleaning, and ion milling. Fig. 3 shows that some very fine Si crystallites with sizes 15-100 Å are embedded in a mesh-like porous structure, which is mainly composed of material with an amorphous phase. These fine particles are more likely to be the quantum structure inside the stained film. By this novel approach, we prove that the appearance of amorphous material is not due to TEM sample preparation artifacts, but probably originates from the degradation of the original crystalline Si (c-Si) after stain etching.

Atomic force microscopy (AFM) was employed to reveal detailed surface topography of PS. Surface profiles of PS samples prepared by conventional anodization, lateral anodization, and stain etching are shown in Fig. 4 [7]. Columnar features are observed in all of the PS sample, with a wide distribution of the pore sizes from thousands to hundreds angstroms. In addition, the surface of the stain-etched PS is apparently smoother than the surface of an anodized sample. Protuberances observed in all of the films with sizes comparable or smaller than 100 Å could be the

light-emitting features, giving the possibility that the quantum-size effect is the major mechanism for the visible PL.

Compositional analysis was performed by secondary ion mass spectroscopy (SIMS) [8]. Very high concentrations of H, C, O, and F species were detected in the PS samples. We believe that the impurity shown in the SIMS spectra come primarily from two sources: the anodization solution and atmospheric exposure. H and F are most likely from the anodization electrolyte since the samples are prepared from HF-based solutions and the others may source from the prolonged exposure to air.

#### **4. PL Mechanism Study**

Several mechanisms have been proposed in the literature to explain the origin of visible PL from PS. The basic mechanisms which have received the most attention are quantum confinement in microcrystalline Si ( $\mu\text{c-Si}$ ), Si-H complexes, and Si-O-H complexes. Within the quantum confinement model are additional PL limiting factors and concepts which may play an important role, including passivation and surface states. A summary of the major luminescence mechanisms is given in Fig. 5.

A series of experiments are designed to investigate the validity of each PL mechanism. For clarity, the mechanisms and limiting factors of PL will be discussed by item as follows.

##### **(1) Quantum confinement in $\mu\text{c-Si}$**

Three approaches have been adopted in this study to examine the role of quantum confinement in PS: directly imaging the quantum feature sizes of the PS luminescent structure by TEM, applying specific processes to reduce the sizes of the quantum structure and then observing the change in PL, and preparing PS from amorphous Si (a-Si) substrates.

As mentioned in the section of "Material Study", the as-prepared PS with H-passivated surface contains very fine Si particles with sizes in the range of 15 to 100 Å [6]. By dry oxidation of a non-luminescent PS sample at 1000°C for 10 min, we directly imaged the quantum particles in O-passivated luminescent PS with lattice resolution by high-resolution TEM. Since negligible H left after the high-temperature oxidation, the appearance of PL from PS after oxidation suggests the irrelevance of H atoms to the observed PL. The sizes of these nanocrystallites are estimated to be 1.5-

4.0 nm, consistent with what we would expect for effective quantum confinement of Si. With an additional oxidation treatment of the sample at 1000°C for 40 min, we showed that the disappearance of the nanocrystallites due to the consumption of Si during oxidation was parallel to the quenching of room-temperature PL. The TEM micrographs are shown in Fig. 6.

The fresh anodized non-luminescent PS was oxidized in 10% O<sub>2</sub>+N<sub>2</sub> ambient at 900°C for 1-48 min to study the development of the PL with oxidation time. The resulting PL is shown in Fig. 7. The peak of the PL intensity monotonically blue-shifts with oxidation time. The inset of Fig. 7 further indicates that, at the beginning, PL intensity increases as more and more crystallites are reduced to appropriate quantum sizes by the oxidation. At 900°C, a complete oxide with good passivation quality is expected to cover the PS surface. This rise in PL intensity is counter to the prediction of Si-H-based or Si-O-H-based mechanisms, since the H amount is negligible and is decreasing with oxidation time. Eventually, as the oxidation continues, the luminescent particles will be totally consumed, which results in the decrease in PL intensity.

Numerous other methods have also been used to reduce the quantum size and produce a net blue-shift of the PL peak. In addition to thermal oxidation, wet chemical oxidation can also be used. Our observations with successive 5s oxidation in HNO<sub>3</sub> followed by deoxidation in 5% HF also indicate that the blue-shift can be readily and rapidly extended into the orange and yellow emission ranges. Fig. 8 shows the PL blue-shift of PS due to chemical oxidation/deoxidation by HNO<sub>3</sub> and HF, respectively.

Stain etching was performed on a structure of 2 μm-thick a-Si/c-Si substrate to investigate the importance of Si crystallites for visible PL from PS [9]. No experimental conditions with a variety of combinations between solution concentration, etching time, and substrate doping can produce luminescent porous a-Si. However, with a brief 4 min N<sub>2</sub> anneal prior to stain etching at temperatures from 550°C to 1150°C, we are able to show that the appearance of visible PL after stain etching coincides with the TEM observation of the recrystallization of a-Si before etching, revealing the critical role of Si crystallites to the observed PL.

## (2) Surface passivation

Two issues have been investigated with respect to the surface passivation of PS. First, the role of H in PL is examined by gradually replacing the surface H passivation with O passivation [10]. This was done by a room-temperature anodic oxidation process. We found that the PL intensity did not track with changes in the silicon hydride peaks at  $\sim 2088\text{ cm}^{-1}$ . On the contrary, the PL increased while the hydride peaks decreased, suggesting that the role of H in PS was more likely the surface passivator instead of an active species directly participating the light-emission process. The result shows that the PL change is mainly determined by other factors, such as a structural change or the density of non-radiative centers, and does not necessarily follow the amount of silicon hydrides in the PS.

The second issue we have investigated is the influence of quality of surface passivation on the PL intensity. This is studied by measurement of the dangling bond (DB) density, a representative of passivation quality, after exposing anodically oxidized PS to different levels of laser irradiation [11]. We found that the increase percentage in PL intensity quantitatively followed the decrease percentage in DB density after laser exposure. The results indicate that the PL intensity is dominated by the amount of DB density, provided that the structural change of PS is negligible. We thereby conclude that the surface passivation is a required but not sufficient condition for efficient visible luminescence from PS.

### (3) Si-H or Si-O-H-based mechanisms

As mentioned previously, many experiments we have done so far show that the Si-H or Si-O-H complexes do not primarily operate in PS, although Brandt *et al.* support that the PL of PS is primarily from siloxene and its derivatives [12]. In order to get more in-depth information, we performed curve fitting for  $\text{Si}_{2p}$  core-level spectra of X-ray photoelectron spectroscopy (XPS) with different anodization time. The  $\text{Si}_{2p}$  spectra have a tendency to shift to the higher energy side with increasing anodization time, as shown in Fig. 9. The spectra were decomposed into 4 different Si oxidizing states, *i.e.* Si(+1), Si(+2), Si(+3), and Si(+4), in order to study the relationship between the individual state and the PL intensity. Based on molecular electronics mechanism, the PL intensity should be proportional to the amount of the active molecules, which may be in any one of the Si oxidizing state. However, Fig. 10 shows that the percentage change of the PL intensity has no quantitative match to

any component of  $\text{Si}_{2p}$  spectra and their combinations, suggesting the unimportance of siloxene and its derivatives to the visible PL of PS.

## 5. EL Devices

### 5.1 Device fabrication

As shown in Fig. 11, two types of EL devices with buried luminescent PS layers were fabricated in this study. Type 1 is the surface-emitting device with a shallow  $p^+/n^-$  junction. Type 2 is an edge-emitting device with a much deeper  $n^+/p^-$  junction. At least two advantages can be obtained by the employment of buried luminescent PS. First, the luminescent layer will receive more protection against the detrimental effects from subsequent processes. Second, burying the luminescent PS can greatly facilitate making electrical contacts to the active PS layer. Much better contact quality is expected due to the lower porosity of the top non-luminescent PS layer. For the formation of shallow  $p^+/n^-$  junction, boron ions were implanted at 5 KeV into 1-10  $\Omega\text{cm}$  As-doped (100)Si at a dose of  $5 \times 10^{14} \text{ cm}^{-2}$ . The resulting dopant profile before and after annealing was checked by spreading resistance profiles (SRP) and secondary ion mass spectroscopy (SIMS). The sample was pre-patterned with positive photoresist prior to the anodization. The anodization was performed with illumination in a typical single-cell setup with the backside metallized to improve the uniformity of the electrical current density.

The fact that the resulting luminescent layer is buried under the top non-luminescent PS can be readily verified by using a hand-held two-band ultraviolet (UV) light source. As shown in Fig. 12, the anodized areas exhibit bright red color under the illumination of 365 nm UV light. However, the same sample shows no visible luminescence under the illumination of 254 nm UV light. The dual band UV experiment indicates that the buried depth in this specific case should be between the absorption depths of 254 nm and 365 nm UV light in the sample. By referring to the optical absorption curve of a comparable sample, we estimate the buried depth to be 230-1000 Å in this case.

An edge-emitting EL device was manufactured by anodizing a deeper  $n^+/p^-$  junction. The junction was formed by counter-doping 4-6  $\Omega\text{cm}$  p-(100)Si wafers with

phosphorus oxychloride ( $\text{POCl}_3$ ). The estimated junction depth is  $\sim 1.6 \mu\text{m}$  by directly observing the stain-etched junction. The anodization was carried out in the dark to prevent the top n-type layer from becoming luminescent after anodization. The resulting PL cannot be imaged under the illumination of UV light.

## 5.2 Device characterization

Fig. 13(a) shows the EL from surface-emitting device, along with the PL photograph of the as-anodized device in Fig. 13(b) for comparison. The turn-on voltage for EL is  $\sim 25 \text{ V}$ , as observed by the naked eye. Compared to the PL of the as-anodized sample, the EL shows an obvious blue-shift from red to red-orange. As also shown in Fig. 13(c), the EL can be pale-green to light-blue if the anodization time is lengthened to longer than 10 min.

The edge-emitting device electroluminesced orange-yellow to the naked eye, as shown in Fig. 14. The device started to show observable EL after the applied voltage exceeded 14 V. Also shown as curve (a) in Fig. 14 is the I-V characteristics for the initial Si  $n^+/p^-$  junction without anodization. Curve (b) in Fig. 14 shows the I-V characteristics of the same junction after anodization at  $10 \text{ mA/cm}^2$  for 5.5 min in the dark. The junction after anodization still exhibited current rectification, although not as good as a typical Si diode. The operating current density of our edge-emitting device is as low as  $4 \text{ mA/cm}^2$ , which is among the lowest of the reported PS-based EL devices [13-18]. The increased efficiency of the device is attributed to the use of p-n junction structure and the buried luminescent PS layer.

## 6. Conclusions

In conclusion, we proposed that the visible PL from PS is due primarily to quantum confinement in Si nanocrystallites. Quantum confinement in PS is supported primarily by the imaging of Si nanocrystallites in PS and the ability to blue-shift the PL by processing designed to reduce quantum feature sizes. Passivation plays a role in eliminating non-radiative recombination channels, thereby increasing the relative radiative recombination efficiency. PL from thermally oxidized PS indicates that the H-based PL mechanisms (including both Si-H and Si-O-H complexes) are not responsible for the visible PL. The approach of using buried luminescent PS layers in

EL devices can be utilized to greatly improve the EL performance.

While luminescent PS holds some promise for Si optoelectronics, process control and film stability continue to be major concerns. One of the great contributions of luminescent PS is the demonstration that quantum confinement can produce efficient visible light emission from Si. Perhaps the future direction is to utilize the concepts learned from PS and develop alternative means of fabricating quantized Si structures, such as CVD-based technologies. Another future direction might be the search for a mid-gap trap site to produce efficient luminescence in the near IR for optical fiber communications.

As for the future development of PS, using O-passivated instead of H-passivated PS for device fabrication may be a feasible way to prevent the stability issue. The increased impedance can probably be compensated by the use of a thinner luminescent PS layer. For a superior electrical contact to PS, low-temperature CVD-deposited metals, such as W, may greatly reduce the contact resistance due to improved penetration into the porous structure.

## 7. References

1. C. Pickering, M. I. J. Beale, D. J. Robbins, P. J. Pearson, and R. Greef, J. Phys. C **17**, 6535 (1984).
2. L. T. Canham, Appl. Phys. Lett. **57**, 1046 (1990).
3. S. Shih, K. H. Jung, T. Y. Hsieh, J. Sarathy, J. C. Campbell, and D. L. Kwong, Appl. Phys. Lett. **60**, 1863 (1992).
4. J. Sarathy, S. Shih, K. H. Jung, C. Tsai, K.-H. Li, D. L. Kwong, J. C. Campbell, S.-L. Yau, and A. J. Bard, Appl. Phys. Lett. **60**, 1532 (1992).
5. S. Shih, C. Tsai, K.-H. Li, K. H. Jung, J. C. Campbell, and D. L. Kwong, Appl. Phys. Lett. **60**, 633 (1992).
6. S. Shih, K. H. Jung, R.-Z. Qian, and D. L. Kwong, Appl. Phys. Lett. **62**, 467 (1993).
7. T. George, M. S. Anderson, W. T. Pike, T. L. Lin, R. W. Fathauer, K. H. Jung, and D. L. Kwong, Appl. Phys. Lett. **60**, 2359 (1992).
8. K. H. Jung, S. Shih, D. L. Kwong, T. George, T. L. Lin, H. Y. Liu, and Zavada, J. Electrochem. Soc. **139**, 3363 (1992).
9. K. H. Jung, S. Shih, D. L. Kwong, C. C. Cho, and B. E. Gnade, Appl. Phys. Lett. **61**, 2467 (1992).
10. S. Shih, K. H. Jung, D. L. Kwong, M. Kovar, and J. M. White, Appl. Phys. Lett. **62**, 1780 (1993).
11. S. Shih, K. H. Jung, J. Yan, D. L. Kwong, M. Kovar, J. M. White, T. George, and S. Kim, Appl. Phys. Lett. **63**, 3306 (1993).
12. M. S. Brandt, H. D. Fuchs, M. Stutzmann, J. Weber, and M. Cardona, Solid State Commun. **81**, 307 (1992).
13. A. Richter, P. Steiner, F. Kozlowski, and W. Lang, IEEE Electron Device Lett. **12**, 691 (1991).
14. N. Koshida and H. Koyama, Appl. Phys. Lett. **60**, 347 (1992).
15. Z. Chen, G. Bosman, and R. Ochoa, Appl. Phys. Lett. **62**, 708 (1993).
16. F. Namavar, H. Paul, and N. M. Kalkhoran, Appl. Phys. Lett. **60**, 2514 (1992).
17. T. Futagi, T. Matsumoto, M. Katsuno, Y. Ohta, H. Mimura, and K. Kitamura,

- Jpn. J. Appl. Phys. **31**, L616 (1992).
18. P. Steiner, F. Kozlowski, and W. Lang, Appl. Phys. Lett. **62**, 2700 (1993).

## 8. Publication Lists

1. S. Shih, K. H. Jung, T. Y. Hsieh, J. Sarathy, C. Tsai, K.-H. Li, J. C. Campbell, D. L. Kwong, and T. L. Lin, "Photoluminescence and structure of chemically etched porous Si and laterally anodized porous Si", *Mater. Res. Soc. Symp. Proc.* **256**, pp. 27-30, Boston, U. S. A. (1991).
2. K. H. Jung, S. Shih, T. Y. Hsieh, J. C. Campbell, D. L. Kwong, T. George, T. L. Lin, H. Y. Liu, J. Zavada, and S. Novak, "Structure and composition of luminescent laterally anodized porous Si", *Mater. Res. Soc. Symp. Proc.* **256**, pp. 31, Boston, U. S. A. (1991).
3. C. Tsai, K.-H. Li, J. Sarathy, K. H. Jung, S. Shih, B. K. Hance, J. M. White, D. L. Kwong, P. R. Sharps, M. L. Timmons, R. Venkatasubramanian, J. A. Hutchby, and J. C. Campbell, "The role of silicon monohydride and dihydride in the photoluminescence of porous silicon and photoluminescence of porous silicon buried underneath epitaxial GaP", *Mater. Res. Soc. Symp. Proc.* **256**, pp. 203, Boston, U. S. A. (1991).
4. S. Shih, K. H. Jung, and D. L. Kwong, "Structural investigation of photoluminescent porous Si by transmission electron microscopy", *Mater. Res. Soc. Symp. Proc.* **281**, pp. 513, Boston, U. S. A. (1992).
5. K. H. Jung, S. Shih, D. L. Kwong, C. C. Cho, and B. E. Gnade, "Visible PL and microstructure of annealed and chemically etched amorphous Si", *Mater. Res. Soc. Symp. Proc.* **283**, pp. 33, Boston, U. S. A. (1992).
6. C. Tsai, K.-H. Li, J. Sarathy, S. Shih, J. C. Campbell, B. K. Hance, and J. M. White, "Thermal treatment studies of the photoluminescence intensity of porous silicon", *Appl. Phys. Lett.* **59**, pp. 2814 (1991).
7. K. H. Jung, S. Shih, T. Y. Hsieh, D. L. Kwong, and T. L. Lin, "Intense Photoluminescence from laterally anodized porous Si", *Appl. Phys. Lett.* **59**, pp. 3264 (1991).
8. S. Shih, C. Tsai, K.-H. Li, K. H. Jung, J. C. Campbell, and D. L. Kwong, "Control of porous Si photoluminescence through dry oxidation", *Appl. Phys. Lett.* **60**, pp. 633 (1992).
9. J. Sarathy, S. Shih, K. H. Jung, C. Tsai, K.-H. Li, D. L. Kwong, J. C.

- Campbell, S.-L. Yau, and A. J. Bard, "Demonstration of photoluminescence in nonanodized silicon", *Appl. Phys. Lett.* **60**, pp. 1532 (1992).
10. S. Shih, K. H. Jung, T. Y. Hsieh, J. Sarathy, J. C. Campbell, and D. L. Kwong, "Photoluminescence and mechanism of chemically etched silicon", *Appl. Phys. Lett.* **60**, pp. 1863 (1992).
  11. K. H. Jung, S. Shih, D. L. Kwong, C. C. Cho, and B. E. Gnade, "Visible photoluminescence from porous Si formed by annealing and chemically etching amorphous Si", *Appl. Phys. Lett.* **61**, pp. 2467 (1992).
  12. K. H. Jung, S. Shih, D. L. Kwong, T. George, T. L. Lin, H. Y. Liu, and Zavada, "Photoluminescence, structure, and composition of laterally anodized porous Si", *J. Electrochem. Soc.* **139**, pp. 3363 (1992).
  13. K.-H. Li, C. Tsai, S. Shih, T. Hsu, D. L., Kwong, and J. C. Campbell, "The photoluminescence spectra of porous Si boiled in water" *J. Appl. Phys. Communications* **72**, pp. 3816 (1992).
  14. S. Shih, K. H. Jung, R.-Z. Qian, and D. L. Kwong, "Transmission electron microscopy study of chemically etched porous Si", *Appl. Phys. Lett.* **62**, pp. 467 (1993).
  15. S. Shih, K. H. Jung, D. L. Kwong, M. Kovar, and J. M. White, "Effects of H and O passivation on photoluminescence from anodically oxidized porous Si layers", *Appl. Phys. Lett.* **62**, pp. 1780 (1993).
  16. S. Shih, K. H. Jung, D. L. Kwong, M. Kovar, and J. M. White, "Photoluminescence study of anodized porous Si after HF vapor phase etching", *Appl. Phys. Lett.* **62**, pp. 1904 (1993).
  17. S. Shih, K. H. Jung, J. Yan, D. L. Kwong, M. Kovar, J. M. White, T. George, and S. Kim, "Photoinduced luminescence enhancement from anodically oxidized porous Si", *Appl. Phys. Lett.* **63**, pp. 3306 (1993).
  18. K. H. Jung, S. Shih, and D. L. Kwong, "Developments in luminescent porous Si", *J. Electrochem. Soc.* **140**, pp. 3046 (1993).
  19. J. Yan, S. Shih, K. H. Jung, D. L. Kwong, M. Kovar, J. M. White, B. E. Gnade, and L. Magel, "Study of thermal oxidation and nitrogen annealing of luminescent porous Si", *Appl. Phys. Lett.* **64**, pp. 1374 (1994).

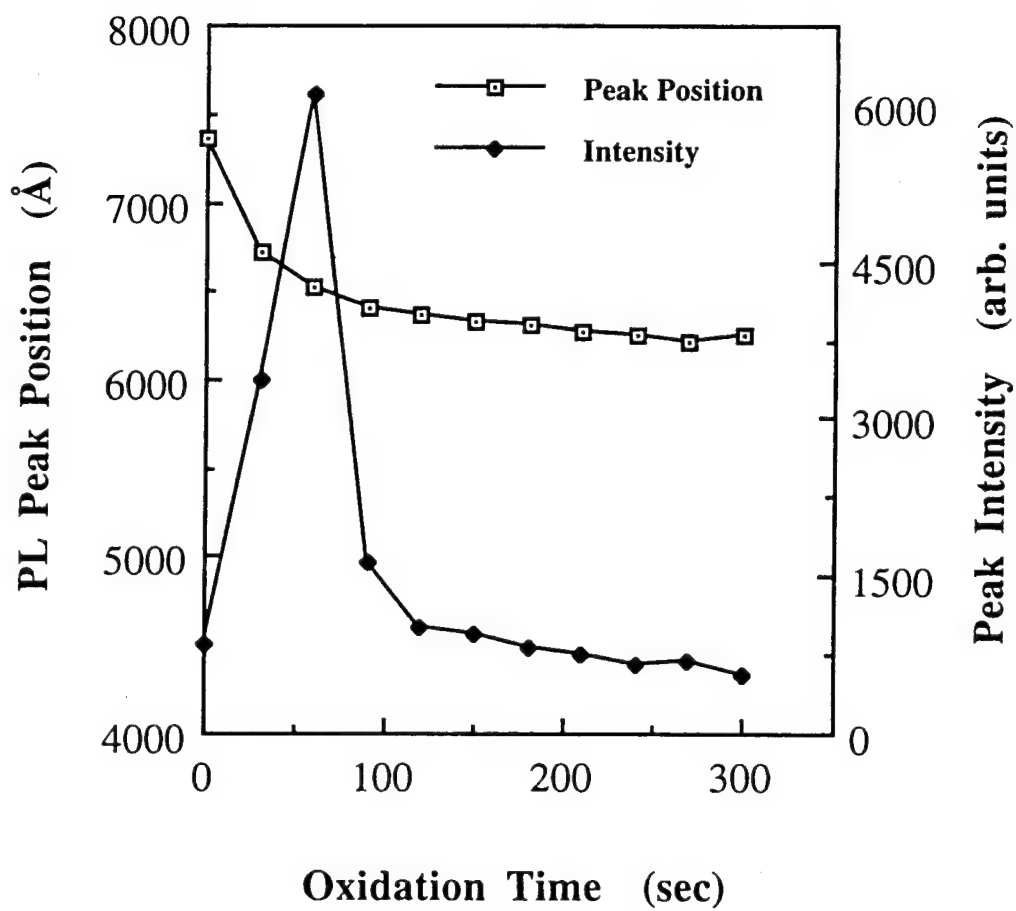


Fig. 1 Measured room-temperature photoluminescence spectral peak and peak intensity as a function of 700°C oxidation time.

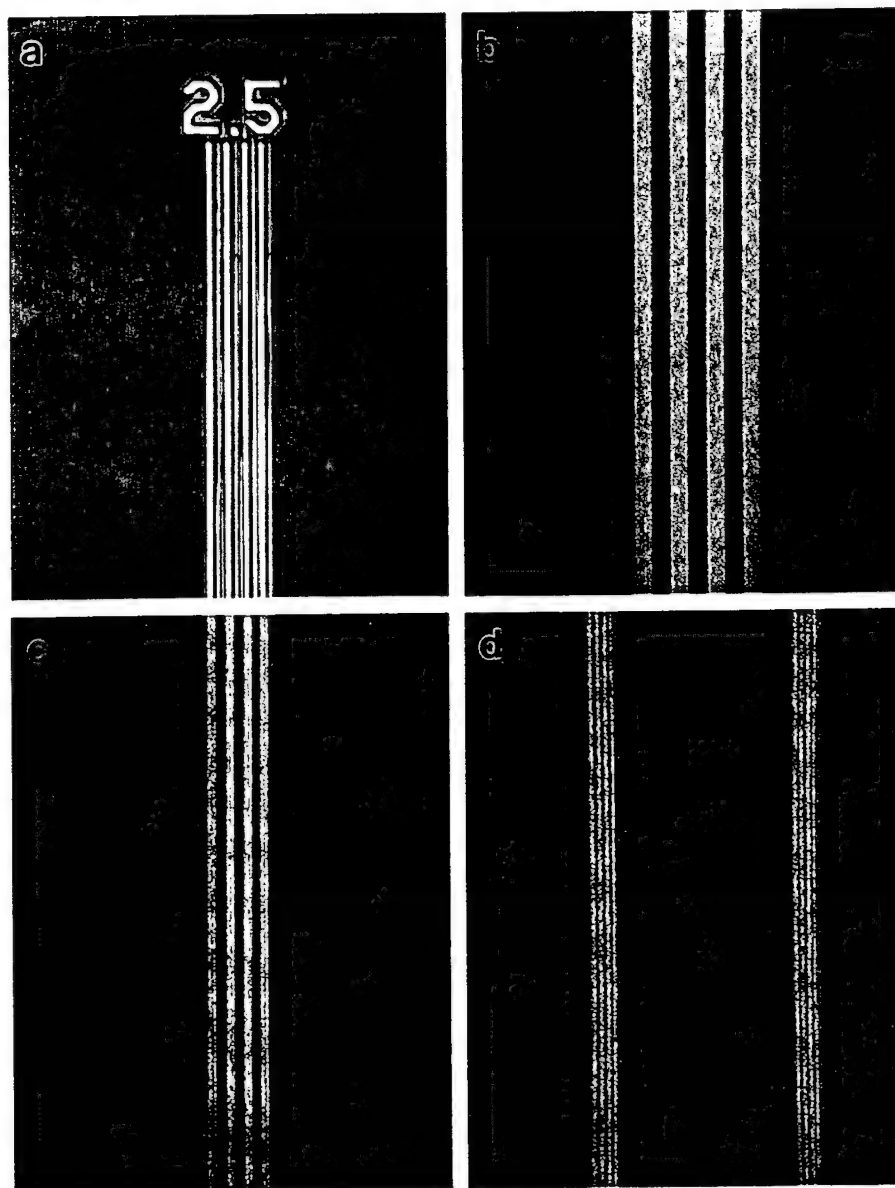


Fig. 2 (a) Optical micrograph of the starting nitride line-patterned Si sample for linewidth of 25  $\mu\text{m}$  and PL micrographs after anodization for linewidths of (b) 250  $\mu\text{m}$ , (c) 25  $\mu\text{m}$ , and (d) 10  $\mu\text{m}$  (left) and 9  $\mu\text{m}$  (right).

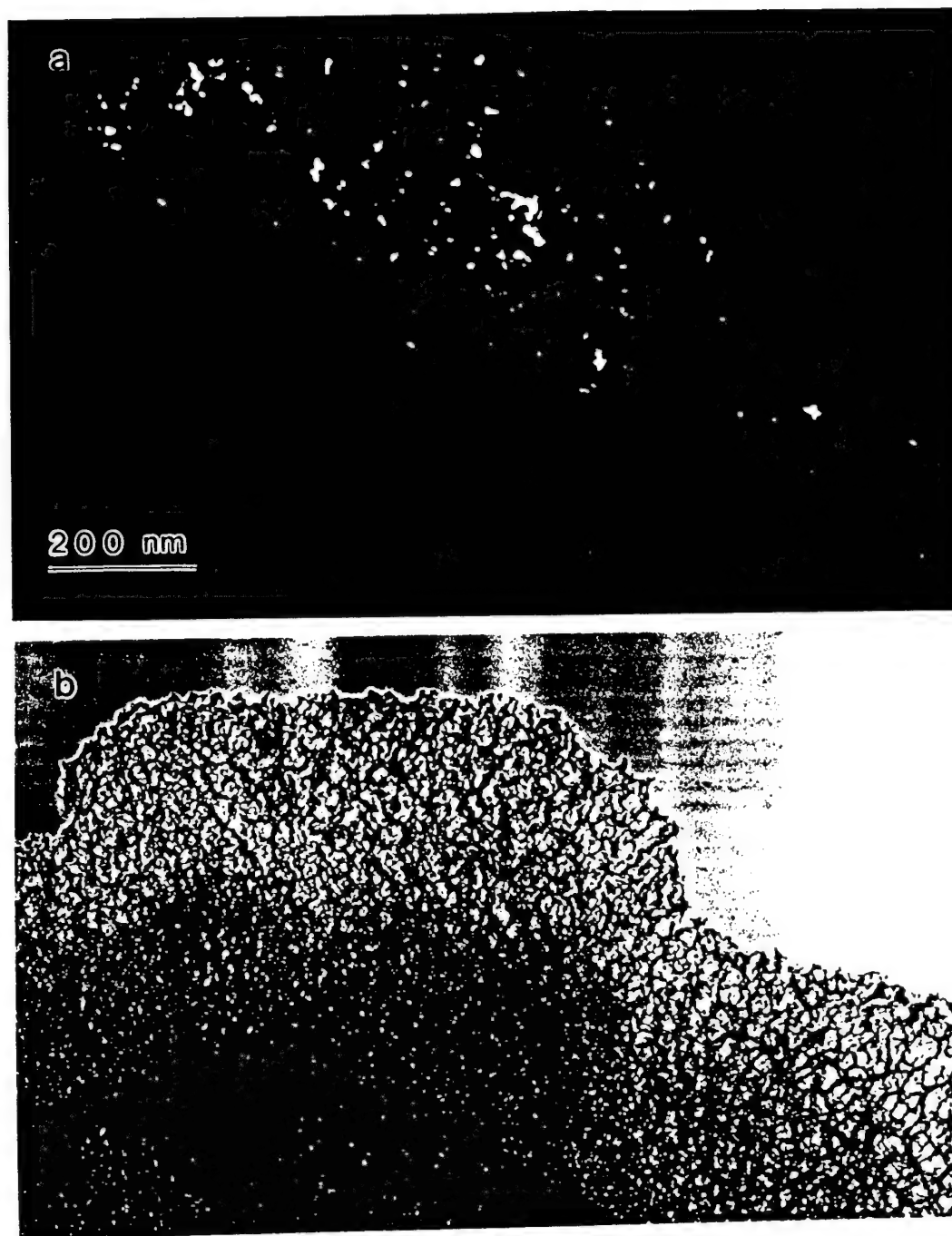
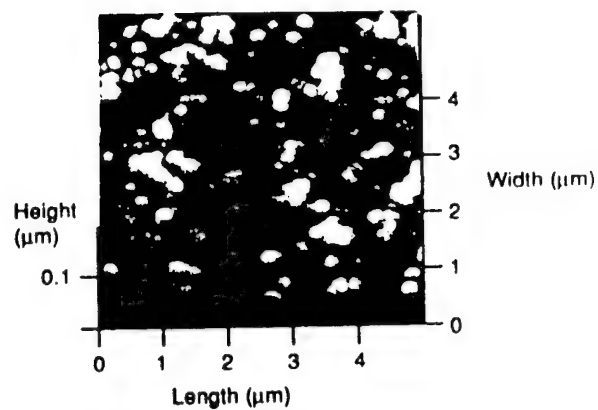
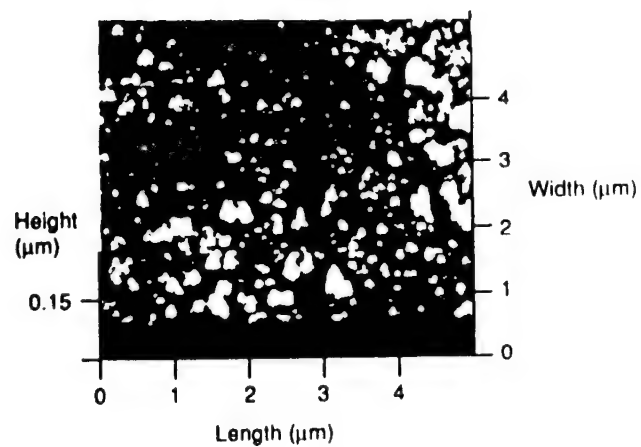


Fig. 3 (a) Dark field and (b) bright field plan-view TEM micrographs showing nanocrystallite sizes in the range of 15~100 Å.

Conventionally-  
Anodized



Laterally-  
Anodized



Stain-etched

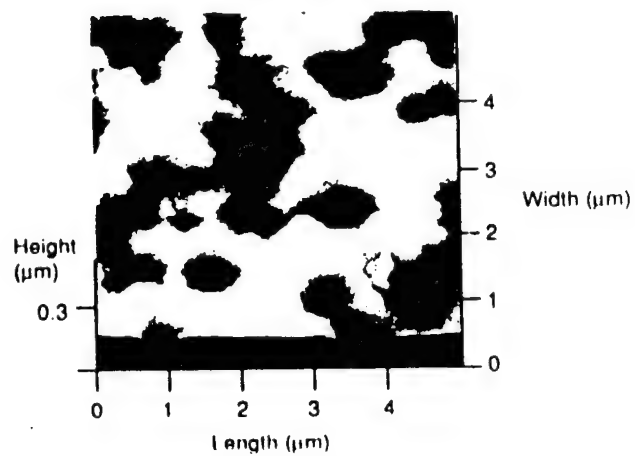


Fig. 4 AFM profile images of (a) a conventional anodized sample, (b) a lateral anodized sample, and (c) a stain-etched sample.

<b>Mechanism</b>	<b>Evidence</b>	<b>Issues Under Debate</b>
Quantum Confinement in c-Si or $\mu$ c-Si	<ul style="list-style-type: none"> <li>• quantum sizes observed by Raman and TEM</li> <li>• PL blue-shifts with process designed to reduce feature sizes</li> <li>• <math>\mu</math>c-Si is known to luminesce</li> </ul>	<ul style="list-style-type: none"> <li>• lack of depth/spatial information in TEM evidence</li> <li>• PL blue-shift doesn't always happen</li> <li>• light-emitting areas are primarily amorphous</li> </ul>
Passivation	<ul style="list-style-type: none"> <li>• trends in PL match dangling bond density</li> </ul>	<ul style="list-style-type: none"> <li>• change in dangling bond density too small</li> </ul>
Surface States	<ul style="list-style-type: none"> <li>• theoretical calculations</li> <li>• fast/slow PL components</li> </ul>	<ul style="list-style-type: none"> <li>• no guarantee surface states will be radiative</li> <li>• explainable by quantum confinement model</li> </ul>
Si-H Complexes	<ul style="list-style-type: none"> <li>• trends in PL intensity and <math>\text{SiH}_2</math> concentration match</li> <li>• PSL similar to <math>\text{SiH}_x</math> or <math>(\text{SiH}_2)_n</math></li> </ul>	<ul style="list-style-type: none"> <li>• <math>\text{SiH}_2</math> and PL changes don't perfectly coincide</li> <li>• oxidized PSLs luminesce</li> </ul>
Si-O-H Complexes (Molecular Electronics)	<ul style="list-style-type: none"> <li>• numerous strong parallels between PSLs and siloxene: FTIR, PL Chemiluminescence Laser ionization <math>\mu</math>-analysis</li> </ul>	<ul style="list-style-type: none"> <li>• slightly different response to annealing conditions</li> <li>• PSL can luminesce without H</li> </ul>

Fig. 5 Summary of proposed luminescence mechanisms.

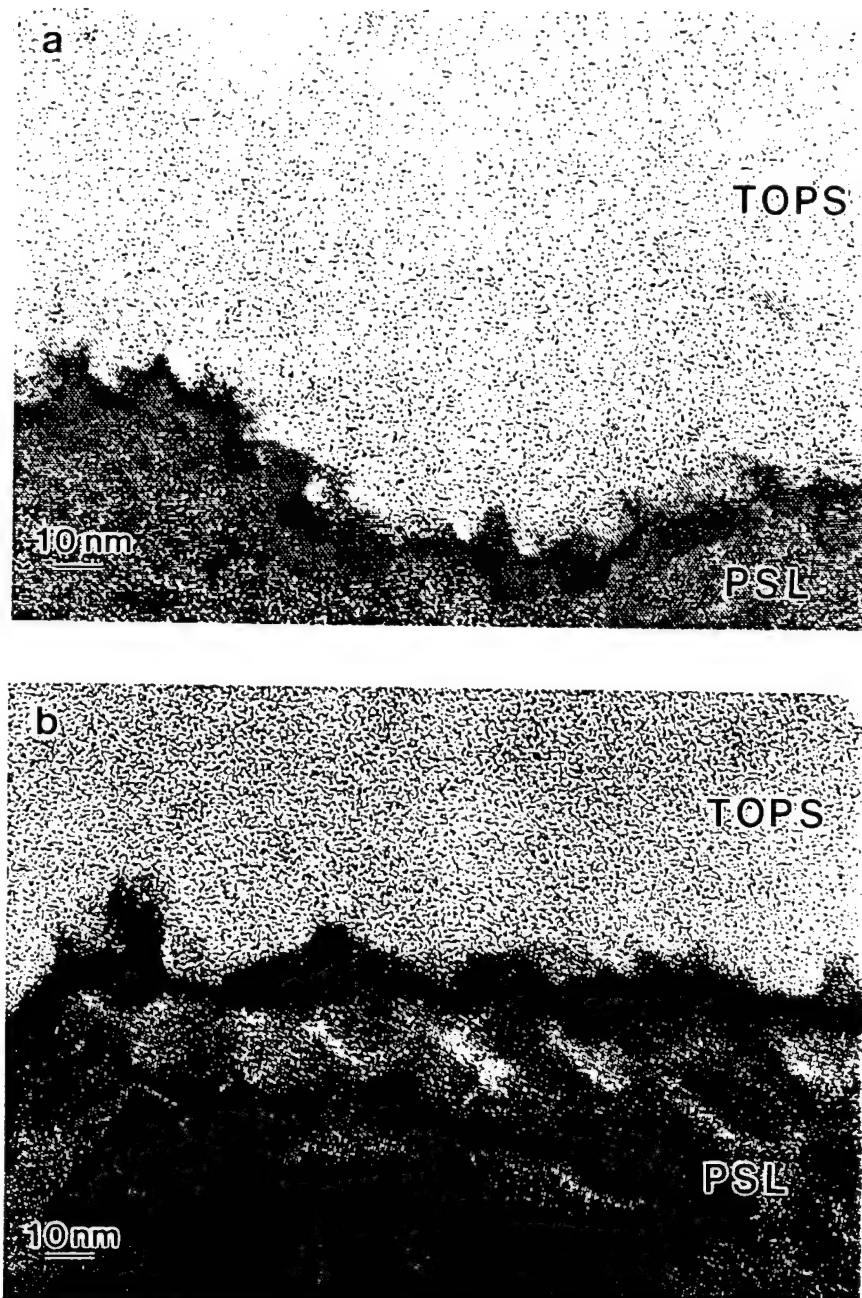


Fig. 6 Cross-sectional TEM micrographs of the thermally oxidized porous Si (TOPS) sample (a) before and (b) after annealing at 1000°C in N<sub>2</sub> for 40 min.

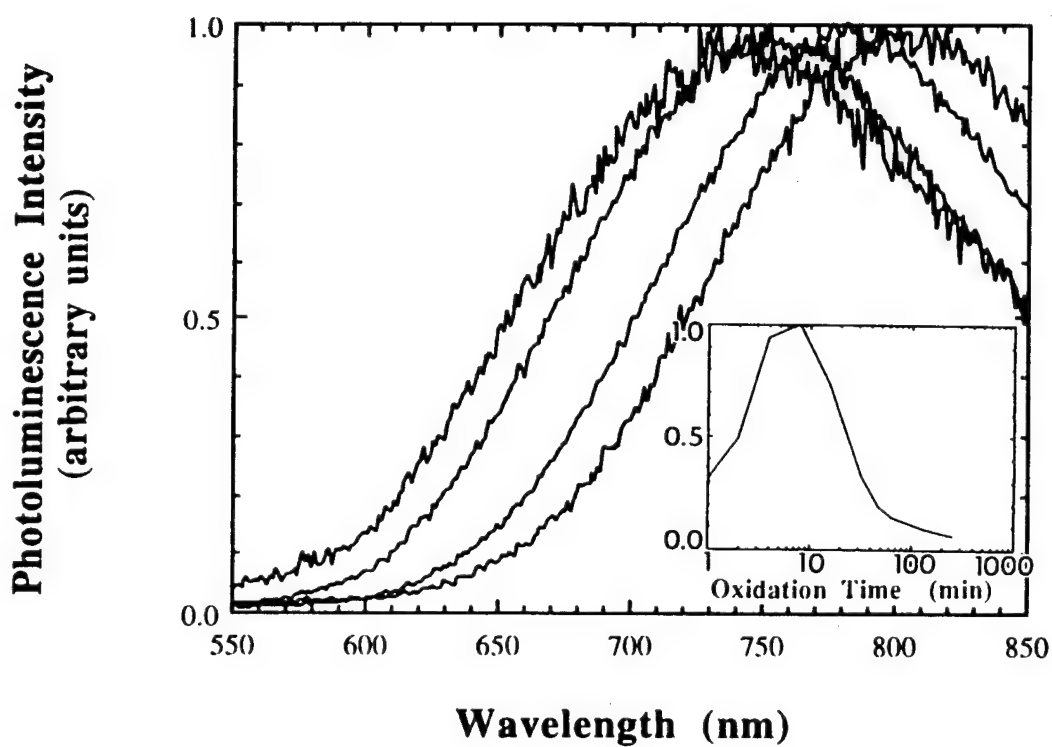


Fig. 7 From right to left, evolution of room-temperature photoluminescence for as-anodized PS after thermal oxidation in 10%  $O_2+N_2$  at 900°C for 1, 4, 16, 48 min. The inset shows the change in PL integrated intensity versus oxidation time.

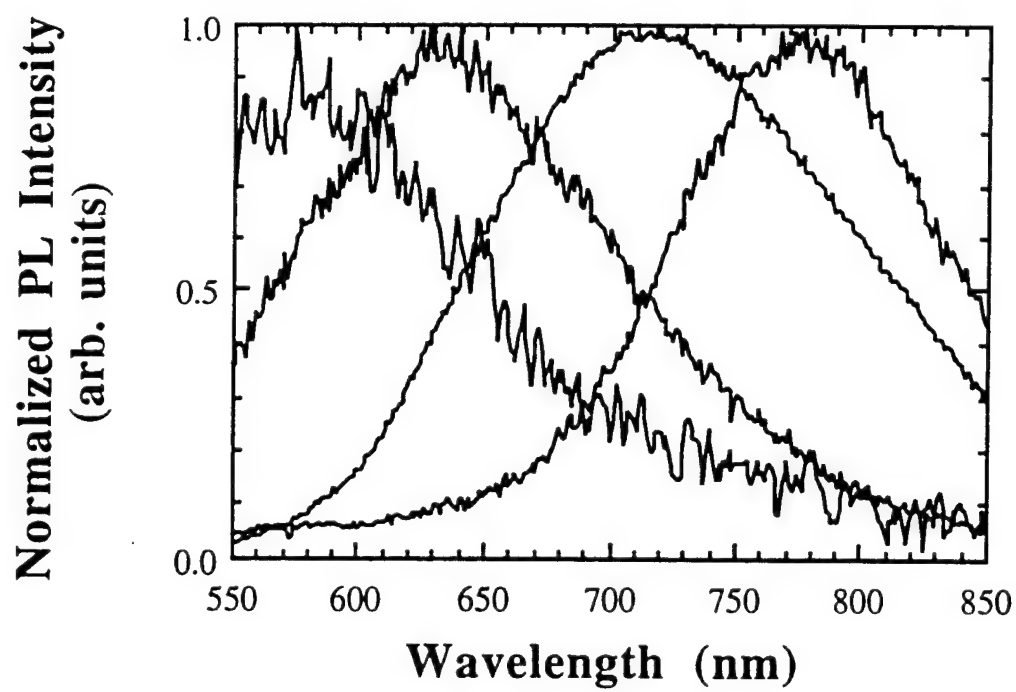


Fig. 8 PL peak shift per cycle of 30s  $\text{HNO}_3$  oxidation followed by a 60s HF deoxidation. Spectra from right to left were taken with increasing times of cycles.

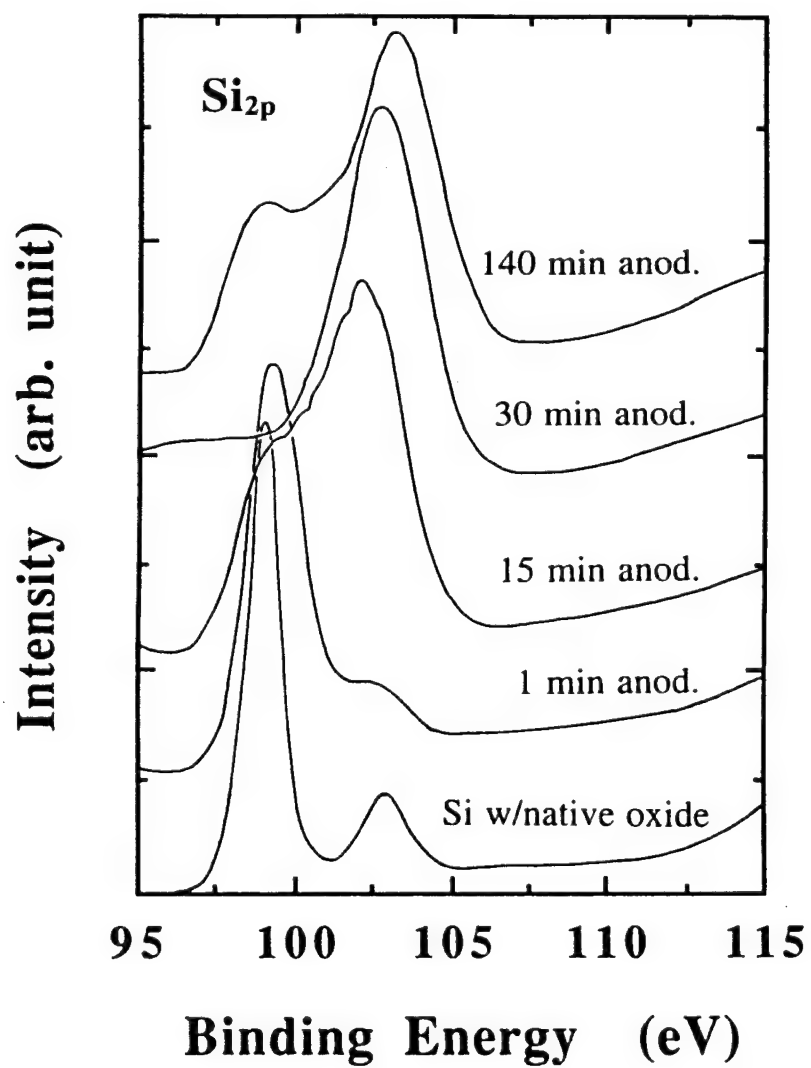


Fig. 9 Evolution of Si<sub>2p</sub> core-level spectra of XPS for porous Si samples with increasing anodization time.

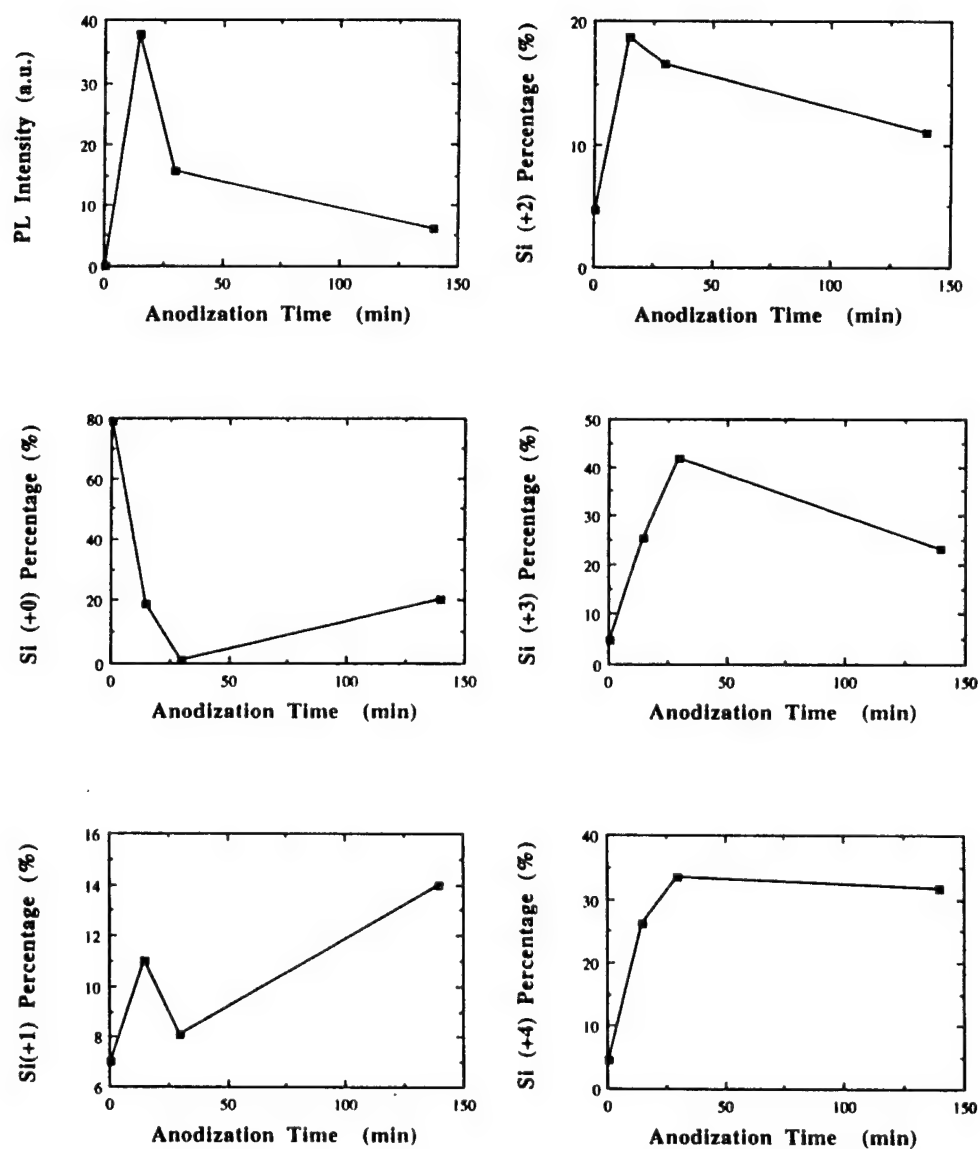
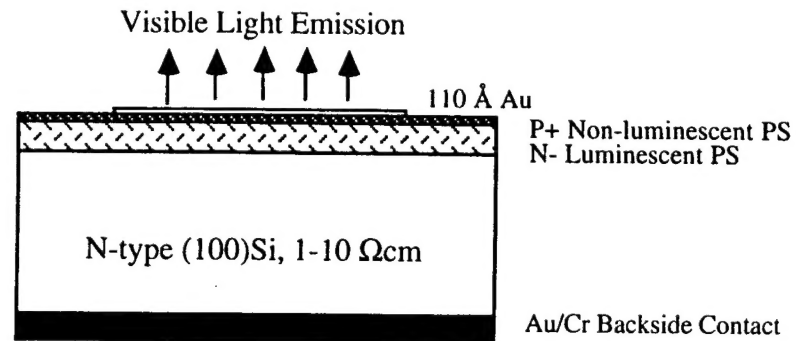


Fig. 10 Percentage change of photoluminescence intensity and each component of  $\text{Si}_{2p}$  spectra with increasing anodization time.

(a) Surface-emitting EL Device



(b) Edge-emitting EL Device

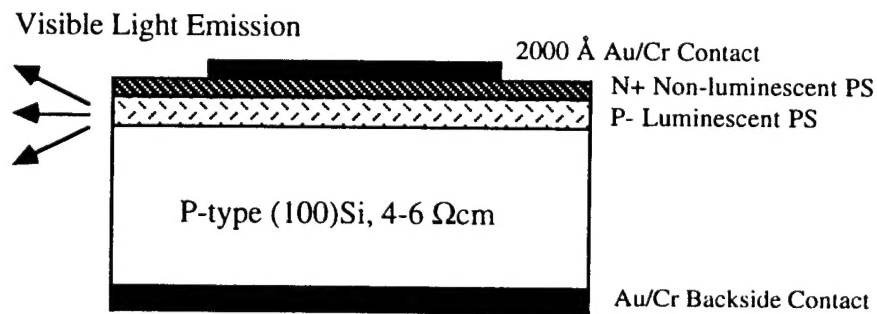
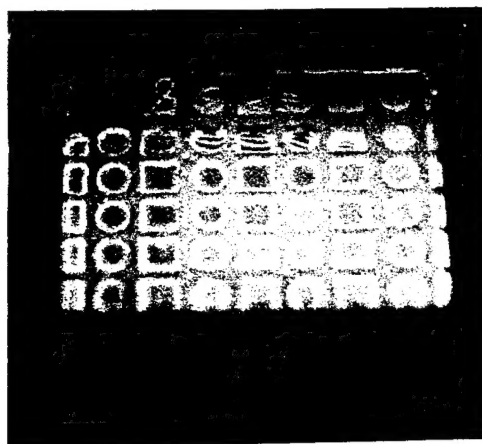


Fig. 11 Schematics of the desired EL device structures. For both the surface-emitting device (a) and the edge-emitting device (b), the luminescent PS layers are buried under the top non-luminescent PS.

(a) Under 365 nm UV illumination



(b) Under 254 nm UV illumination

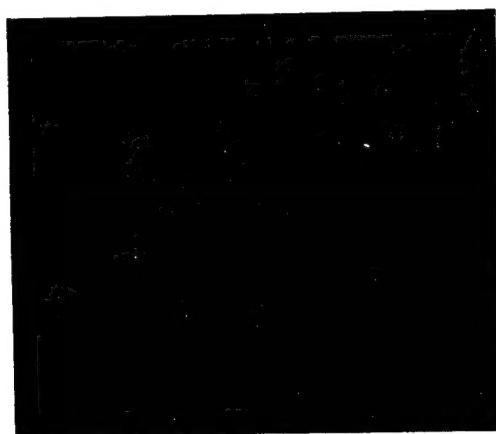
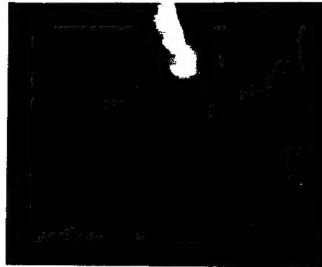
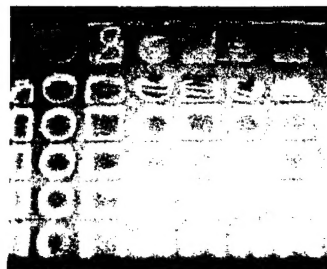


Fig. 12 PL photographs of the fabricated surface-emitting EL device under illumination of (a) 365 nm UV light and (b) 254 nm UV light.

(a) Red-orange EL of a surface-emitting device



(b) PL of the surface-emitting device in (a)



(c) Green-blue EL of a surface-emitting device



Fig. 13 (a) Red-orange EL of the fabricated surface-emitting device; (b) PL of the as-anodized device under 365 nm UV illumination; (c) green to blue EL from a device with an anodization time longer than 10 min.

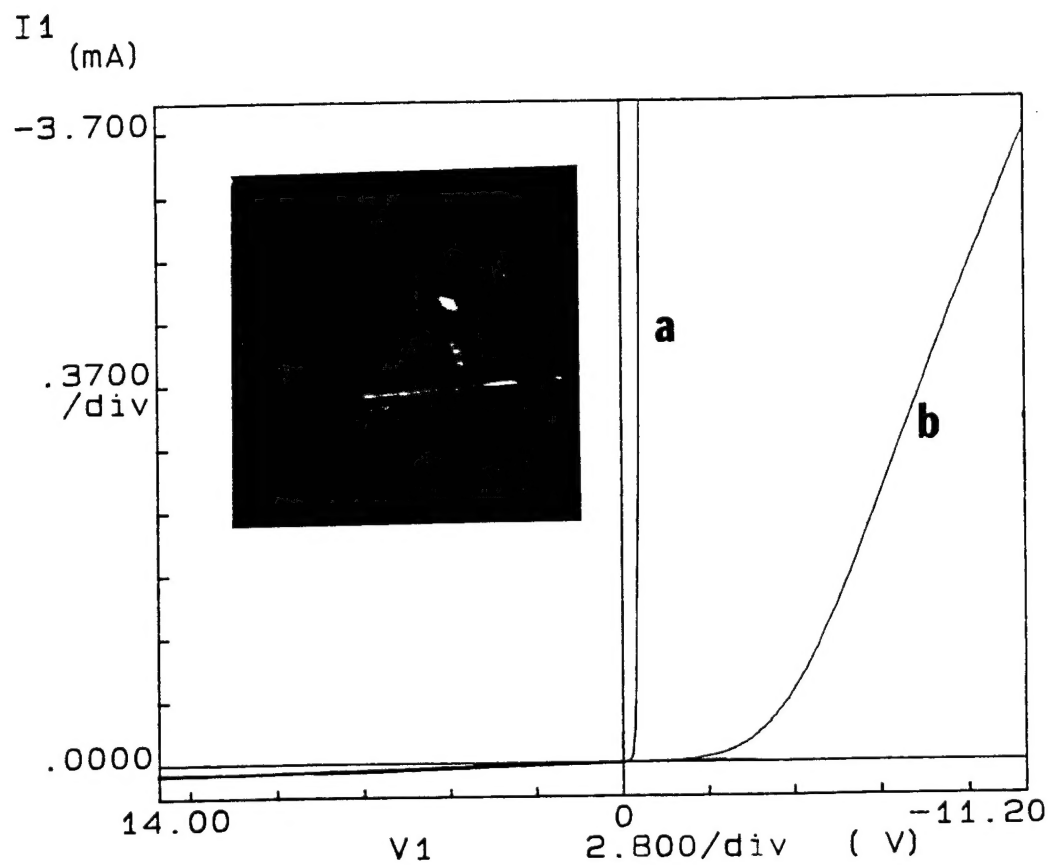


Fig. 14 EL as well as the I-V characteristics of the edge-emitting device. Curve (a) is from the  $n^+/p^-$  junction before anodization. Curve (b) is from the junction after anodization.